HHS Public Access

Author manuscript

J Mater Chem B Mater Biol Med. Author manuscript; available in PMC 2018 September 07.

Published in final edited form as:

J Mater Chem B Mater Biol Med. 2017 September 7; 5(33): 6740–6751. doi:10.1039/C7TB01086A.

Multifunctional $Cu_{39}S_{28}$ Hollow Nanopeanuts for *In Vivo* Targeted Photothermal Chemotherapy

Lihua Li[a,b], **Xianfeng Yang**[a], **Xiaoming Hu**[b], **Yao Lu**[b], **Liping Wang**[a], **Mingying Peng**[a,*], **Hong Xia**[b], **Qingshui Yin**[b], **Yu Zhang**[b,*], and **Gang Han**[c,*]

[a]The China-Germany Research Center for Photonic Materials and Device, the State Key Laboratory of Luminescent Materials and Devices, and Guangdong Provincial Key Laboratory of Fiber Laser Materials and Applied Techniques, the School of Materials Science and Engineering, South China University of Technology, 381 Wushan Road, Guangzhou 510641, China

[b]Guangdong Key Lab of Orthopedic Technology and Implant, Department of Orthopedics, Guangzhou General Hospital of Guangzhou Military Command, 111 Liuhua Road, Guangzhou, Guangdong 510010, China

[c]Department of Biochemistry and Molecular Pharmacology, University of Massachusetts Medical School, Worcester, Massachusetts 01605, United States

Abstract

Actively targeted hollow nanoparticles may play key roles in precise anti-cancer therapy. Here, unique $Cu_{39}S_{28}$ hollow nanopeanuts (HNPs) were synthesized *via* a facile one-step method and the formation mechanism was illustrated. The as-synthesized $Cu_{39}S_{28}$ HNPs exhibit outstanding photothermal conversion efficiency (41.1%) and drug storage capacity (DOX, 99.5 %). At the same time, the DOX drug loading nanocomposites have shown great sensitive response of release to either pH value or near infrared ray (NIR). In particular, the folic acid (FA) can easily conjugate with the synthesized $Cu_{39}S_{28}$ HNPs without further modification to get a targeted effect. The FA modified $Cu_{39}S_{28}$ HNPs showed an efficiently targeting effect *in vitro* and could considerably enhance the tumor-targeting effect more than 10 times *in vivo*. Moreover, the synthetical hyperthermia and drug release from $Cu_{39}S_{28}$ HNPs when under 808 nm laser could significantly improve the therapeutic efficacy compared with photothermal or chemotherapy alone both *in vitro* and *in vivo*. The histological studies in main organs also proved the well biocompatibility, while the tumor sites were in seriously destruction due to the accumulation of the nanocomposites and the combined photothermal chemo therapy effect. Therefore, the multi-functional nanocomposites is excellent antitumor agents due to their superb therapy effect in breast cancer.

TOC image

This work represents a one-step directly aqueous method to synthesize $Cu_{39}S_{28}$ hollow nanopeanuts towards ultrasensitive tumor targeted photothermal chemotherapy.

*Correspondence author: Mingying Peng (pengmingying@scut.edu.cn); Yu Zhang, Yu Zhang (luck_2001@126.com); Gang Han (gang.han@umassmed.edu).

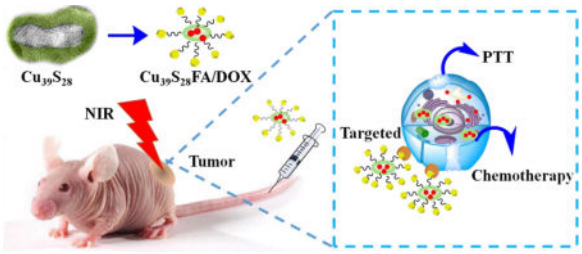

1. Introduction

Breast cancer has become the most lethal illness and common cancer for women in the world.[1] About 248,620 breast cancer patients newly diagnosed in 2011 in China and the 5-year survival rate is 73.1 %, which continues to be a major health and financial burden to women and families.[2] Generally, breast-conversing surgery has become the main treatment choice for women in early breast cancer.[3] Numerous new therapies have entered clinical trials in recent years, radiofrequency ablation (RFA) combined with chemotherapy is considered to be a common approach for early breast cancer treatment. However, there are still many difficulties, such as thermal injury to surrounding normal tissues and increase the new cancer lesions opportunities during conventional RFA, toxicity from high chemotherapeutic drug concentrations, side effects and multidrug resistance of chemotherapy. Therefore, it is necessary to develop new approaches with less invasive and more effective methods to treat breast cancer. With the development of nanomedicine, many new treatment approaches have emerged,[4–6] such as enhanced photodynamic,[4] microwave irradiation,[7] radiotherapy[8] and photothermal therapy[9] induced by various nanoparticles. Among these approaches, photothermal therapy (PTT) is an attractive alternative treatment for cancer therapy, especially for solid tumors, and it usually employs photothermal agents to ablate cancer cells without damaging the surrounding tissues under near infrared ray (NIR) radiation.[10] An ideal photothermal agent should satisfy the following requirements: strong absorbance in the NIR region (700~1300 nm), high photothermal conversion efficiency and good biocompatibility.[11] Fortunately, with the development of nanomaterials and nanotechnology, a wide range of nanomaterials with strong optical absorption in the NIR tissue transparency window, such as noble metal nanostructures,[12–14] semiconductors,[7,8] carbon composites[9,10] and organic nanoparticles,[15, 16] have been developed as photothermally active agents.

Recently, CuS nanoparticles are especially attractive for cancer photothermal ablation due to their low cost and high stability. Chen et al.[17] have developed CuS nanoparticles as photothermal agent for ablation of cancer *in vitro* and *in vivo* under 24 W/cm^2. To enhance the photothemal effect, Hu et al.[18] have synthesized a series of copper chalcogenides including plate-like (70 nm) Cu_9S_5 with photothermal conversion (PTC) of 25.7%and cysteine capped CuS nanoparticles with increasing PTC efficiency up to 38% for ablation of tumor.[19] Moreover, except the photothermal effect, engineering nanoparticles with biocompatible, active tumor targeting and drug delivery effect must be considered. Zha et al. conjugated DOX to gelatin as drug model and then reacted with $CuCl_2$ to get 6–10 nm CuS nanoparticles, then used them for photoacoustic imaging, photothermal therapy and enzyme-

responsive chemotherapy.[20] However, the limited drug loading efficiency and targeted effect still need to explore. For the purpose of enhancing drug delivery efficiency, nanomaterials with hollow or porous structures, which present large surface area, low density and high drug loading capacity, have been the research focus of nanomedicine.[21] Various fabrication procedures of hollow/porous structures have been developed, including mesoporous silica coating,[22] templates methods[23] as well as physical/chemical processes based on Kirkendall effect[24], Ostwald ripening[25], chemically induced self-transformation,[26] and so on. However, for mesoporous silica[27] and template methods, they are tedious, present low product yield and have limited drug loading capacity.[28–31] Especially, the complicated surface modification for further conjugation with targeted groups was really exhausted.[31, 32] Thus, developing targeted hollow CuS nanoparticles combine with photothermal and chemotherapy is still challenge and desirable.

The special nature of L-cysteine (Cys) has attracted our great interest for its well biocompatibility and distinctive structure. In this paper, unique $Cu_{39}S_{28}$ hollow nanopeanuts (HNPs) have been synthesized by reaction of $Cu(NO_3)_2$, L-cysteine and Na_2S in one step *via* a wet chemical method. The as-synthesized $Cu_{39}S_{28}$ HNPs can convert NIR to heat efficiently, as well as provide the loading carrier for anticancer drugs. Then, the HNPs conjugated with folic acid (FA) directly to get a targeted therapy effect for breast cancer cells. The as-prepared $Cu_{39}S_{28}$-FA nanocomposites were characterized by various techniques. Interestingly, as a favorable designed drug delivery system, the release of DOX shows a sensitive response to pH or NIR irradiation. Moreover, the anti-cancer effect of this system was tested both *in vitro* and *in vivo*, respectively. The results demonstrated that the combined targeted photothermal-chemo therapy from $Cu_{39}S_{28}$-FA/DOX were much stronger than PTT or chemotherapy alone. Notably, when functionalized with FA, the nanocomposites accumulated less in the liver and the main organs, which can significantly reduce the potential damage to the body. Thus, the novel $Cu_{39}S_{28}$ nanocomposites may be a safe and potential candidate for breast cancer therapy. The schematic outline of this paper is shown in Scheme 1, and the Materials and Methods section has been placed in the Supporting Information.

2. Results and discussions

2.1 Characterization

In this paper, we have synthesized unique hollow $Cu_{39}S_{28}$ nanopeanuts by reacting with $Cu(NO_3)_2$, L-cysteine, Na_2S with the ratio of 4:3:3(90 min). As shown in Figure 1A, the compound $Cu_{39}S_{28}$ crystallizes in a hexahedron structure with the space group of hexahedron with the space group P3*1 (164) and the lattice parameters areα=22.962 Å, b=22.962 Å, c=41.429 Å,V=21843.58 and Z=18. Several well defined characteristic peaks (e.g., (605), (608), (660)) could be well indexed to the $Cu_{39}S_{28}$ crystal phase, as referenced by the standard file JCPDS 36–0380. There were no obvious impure peaks in the synthesized samples. The Cu 2p XPS spectra of as-synthesized nanoparticles was shown in Figure 1B, the Cu $2p_{2/3}$ fitted peaks reveal 2 peaks at 932.2 eV and 933.5 eV, corresponding with Cu^+ and Cu^{2+}, separately. The XPS spectra further indicated the coexistence of Cu^{2+}

and Cu^{+} in the final products, and the results were in accordance with the $Cu_{39}S_{28}$ XRD results.

Then the nitrogen adsorption-desorption isotherm was employed to investigate the structure of the as-synthesized $Cu_{39}S_{28}$ HNPs, as shown in Figure 1C and D, the results indicate the typical character of IV-type isotherms. The BET surface areas of $Cu_{39}S_{28}$ sample are calculated to be 46 m^2/g and the average pore size should be 4.1 nm, the main cavity was 23 nm The big pores (51 nm) are due to the particle stacking of the adjacent cavities, which is also shown in TEM images. Figure 1 E, F show the representative TEM and HRTEM images of $Cu_{39}S_{28}$ HNPs. The as-synthesized $Cu_{39}S_{28}$ nanoparticles are in an average size of 40 nm, peanut shapes can be clearly seen from Figure 1E, F. The selected area electron diffraction (SAED) pattern on the $Cu_{39}S_{28}$ HNPs exhibits a polycrystalline structure of the interplanar $Cu_{39}S_{28}$ crystal (inset images in Figure 1E). Further microstructure was shown in Figure 1F, the interplanar crystal spacing is ~0.31 nm, which is coincide with the lattice spacing of the (605) planes of $Cu_{39}S_{28}$ nanostructures and coincide well with the XRD results.

Moreover, we have investigated the formation mechanism of the $Cu_{39}S_{28}$ hollow nanopeanuts, the former precursors, samples of different reaction times with Na_2S were tested for XPS, XRD and HRTEM separately and the results were shown in Figure S1 and Figure S2, and the detail results and analyses were shown in the Supporting Information. The formation mechanism was deduced as Figure 1G. Initially, the Cu^{2+} reacted with L-cysteine to form Cu(I)cysteine, for the amount of Cys is so small that more than half of Cu^{2+} cations are superfluous in the solution, non-uniform nanoparticles were formed by hydrogen bond from the amino ($-NH_2$) and carboxyl (-COOH) functional groups in cysteine molecules and cysteine ligand. Such a hydrogen bond mediated self-assembly has been found in the cysteine-capped colloidal metal particles and other small molecule systems.[33, 34] Then after the addition of Na_2S, the excess Cu^{2+} inside the particles came out and reacted with Na_2S, and surrounded the initial cysteine-Cu (I) nanoparticles. Therefore, hollow $Cu_{39}S_{28}$ nanopeanuts were formed, which was in according with the XPS and XRD results.

Furthermore, we have investigated the morphology changes by controlling the ratio of $Cu(NO_3)_2$, Cy, Na_2S in the reaction, different shapes of CuS nanocrystals can obtained with various ratios, as shown in Figure S7. When the ratio was 1:0.5:0.5, a serious aggregation was formed, which may inhibit the further biomedical applications (Figure S7D). While with 1:1:1 or 1:2:2, the nanoparticles was bigger than 100 nm, and it will hard to imply as nanocarrier for *in vivo* applications. The $Cu_{39}S_{28}$ HNPs with the ratio of 1:0.75:0.75 were selected as the samples for next experiments.

The absorption spectra and Fourier transform infrared (FTIR) spectra results of $Cu_{39}S_{28}$, FA, $Cu_{39}S_{28}$-FA nanocomposites are shown in Figures 2A and 2B, respectively. There is a peak for FA at 350~400 nm in Figure 2C and almost no obvious absorption peak at 700 to 900 nm region, while there is a strong absorption band for $Cu_{39}S_{28}$ in the NIR region. After conjugated with FA, the UV-Vis spectrum of $Cu_{39}S_{28}$-FA displays enhanced absorption peaks at 350~400 nm and 700~900 nm. In the FTIR spectrum (Figure 2D), the absorption peak of $Cu_{39}S_{28}$ HNPs at 3452 cm^{-1} corresponds to the NH_2/OH in cysteine and the peak at

1621 cm^{-1} is in accordance with the vibration of the carboxyl group (COO^-).[35] The –SH vibrational band at 2551 cm^{-1} totally disappeared for $Cu_{39}S_{28}$ samples, which evidenced the surface binding of cysteine with copper particles *via* the –SH linkage. The FTIR spectrum of $Cu_{39}S_{28}$-FA nanocomposites shows numerous new bonds corresponding to the different chemical groups of FA. The most prominent bands between 1570 and 1700 cm^{-1} correspond to the carboxyl and amide groups. The fact that both $Cu_{39}S_{28}$ and folic acid moieties were conjugated by chemical reaction in $Cu_{39}S_{28}$-FA was evidenced in the absorption intensities at 1605 cm^{-1} and 1693 cm^{-1} for the amide group. In the FA spectrum, the absorption intensities at 1605 cm^{-1} was weaker than at 1693 cm^{-1}. In the $Cu_{39}S_{28}$-FA spectrum, however, the band at 1605 cm^{-1} has a higher intensity than that at 1693 cm^{-1} because of the carboxyl group in $Cu_{39}S_{28}$.

2.2 Photothermal Effect

The temperature changes of gradient concentrations $Cu_{39}S_{28}$ and $Cu_{39}S_{28}$-FA nanocomposites have been measured by a temperature sensor to identify the inherent photothermal effects of $Cu_{39}S_{28}$ HNPs, as shown in Figure 3. Under 0.5 W/cm^2 of 808 nm laser radiation, the temperature change of $Cu_{39}S_{28}$ solutions (1000 μg/mL) reached nearly 24 °C, while only a 3 °C change in pure water was observed. When the laser power was 1 W/cm^2, the highest temperature in $Cu_{39}S_{28}$ solution reached 52 °C, which is sufficient to lead to DNA damage, denaturation and finally result in irreversible cell damage when co-cultured with cancer cells.[11] The maximum temperature for water only reached to 26 °C after 6 min irradiation. The results were similar to these of $Cu_{39}S_{28}$ nanoparticles for the $Cu_{39}S_{28}$-FA nanocomposites. The study on the photostability of $Cu_{39}S_{28}$ nanocavities was also carried out (Figure S3) and the results demonstrated that under continuous irradiation by NIR laser for 1 h, the absorption by $Cu_{39}S_{28}$ had no obvious reduction, indicating good photostability. As expected, the thermal effect is highly dependent on the concentration of $Cu_{39}S_{28}$ in water and laser dose (power density and time). The temperature reached a tumor therapy hyperthermia range,[36] when using 250 μg/mL $Cu_{39}S_{28}$ HNPs in 808 nm laser at 1 W/cm^2 for 10 min. However, only a slight temperature change (3 °C) of pure water was observed. The temperature reached a tumor therapy hyperthermia range,[36] when using 250 μg/mL $Cu_{39}S_{28}$ HNPs in 808 nm laser at 1 W/cm^2 for 10 min. The photothermal conversion efficiency (η) of $Cu_{39}S_{28}$ (250 μg/mL) is calculated to be 41.1 % (the details and results were shown in Supporting Information and Figure S4). This temperature change under the same power density is relatively high compared to the previously reported mesoporous silica coated CuS nanoparticles (temperature change of 6 °C),[30] indicating the $Cu_{39}S_{28}$ HNPs can convert the NIR light to heat more efficiently without a silica core. At the same time, the synthesis process is really simple and practicable when compared with the core-shell methods.[37, 38] The noble $Cu_{39}S_{28}$ HNPs are proven to be excellent PTT candidates due to the above experiments.

2.3 Drug loading and release

The $Cu_{39}S_{28}$ HNPs not only supports PTT effect, but also may be developed as an ideal drug carrier. The anticancer drug DOX was selected as the loading drug for its good therapy effect in breast cancer.[39] The significant decrease of the DOX absorption at 482 nm (Figure 4A) shows that the DOX was successfully loaded in the hollow nanostructures with physical

adsorption. The $Cu_{39}S_{28}$ HNPs could encapsulate a high dose of DOX up to 99.5 % and the loading content is 49.75 wt. %. The release rate of DOX from $Cu_{39}S_{28}$-FA/DOX in pH 5 and 7.4 PBS buffer was evaluated to simulate the neutral environment of blood circulation and the acidic environment in cancer endosomes, respectively. At room temperature, the DOX-loaded $Cu_{39}S_{28}$-FA remained loaded at pH 7.4, and only less than 10 % DOX was released in 24 h. In pH 5.0 buffer, DOX was quickly released to 32 % of the original amount in the first 8 h, and ~45% in 24 h. This pH responsive controlled-release property can be attributed to the dissociation of electrostatic interaction between the positively-charged DOX molecules and negatively-charged $Cu_{39}S_{28}$-FA HNPs, due to the weak electrostatic interaction of DOX with COO^- and the enhanced solubility of DOX under lower pH environment.[40–42] The $Cu_{39}S_{28}$-FA HNPs can effectively leak DOX during the blood circulation and increase the delivery efficacy in cancer cells. Moreover, the release profiles at 37 °C was also tested (Figure S5), which was a reflection of actual physiological environment. A 90% release of DOX in 48 h was found, which was much higher than at room temperature, indicating the DOX release was temperature responsive and more appropriate for the treatment *in vivo*.

At the same time, the DOX release curve was tested under NIR irradiation in an acidic solution (pH=5). As shown in Figure 4C, under NIR irradiation, with the temperature rising, there was a quick release of DOX in the first 10 min. After turning off the NIR laser, the temperature returned back to room temperature and the DOX release slowed. The irradiation process was repeated at 100 to 110 min and the same quick release occurred. These results confirmed that the release of DOX from $Cu_{39}S_{28}$-FA HNPs could be triggered by NIR laser, due to the photothermal effect of $Cu_{39}S_{28}$-FA/DOX composites. The as-synthesized nanocomposites have a great potential in cancer therapy due to their pH and NIR responsive nature.

2.4 Cell proliferation, PTT and targeted-chemotherapy effects *in vitro* and blood biocompatibility

As discussed above, the synthesized $Cu_{39}S_{28}$ and $Cu_{39}S_{28}$-FA HNPs have an excellent photothermal effect and good drug delivery ability. For further biomedical application, it is necessary to investigate the potential toxicity of these nanocomposites.

First, the standard MTT cell assay was carried out on MCF-7 cells to detect the short-term viability of different nanocomposites. Figures 5A, B show the viability of $Cu_{39}S_{28}$ and $Cu_{39}S_{28}$-FA on MCF-7 cells for concentrations of $Cu_{39}S_{28}$ from 7.8 μg/mL to 1000 μg/mL. The MCF-7 cells are in a good growth status with nanoparticle concentrations from 7.8 to 250 μg/mL, while at the high concentrations of 500 or 1000 μg/mL, the $Cu_{39}S_{28}$ HNPs show little toxic effects on MCF-7 cells. After conjugated with FA, the MCF-7 cells are in a better status at the concentration of 500 μg/mL, which may due to the favorable biocompatibility of FA. From the point of both biocompatibility and photothermal effects, the optimum concentration of 250 μg/mL $Cu_{39}S_{28}$ was selected for the following experiments.

Furthermore, we have also investigated the cell viability on normal cells, mouse fibroblast L929 cells. After co-cultured with different $Cu_{39}S_{28}$ and $Cu_{39}S_{28}$-FA concentrations for 24 h, the same MTT procedure was carried out as MCF-7 cells. As shown in Fiugre S8, there

was no toxicity of the as-synthesized HNPs on L929 cells even with the concentration up to 1 mg/mL. The resluts further confirmed the excellent biocompatiblity of the $Cu_{39}S_{28}$ and $Cu_{39}S_{28}$-FA.

Moreover, to investigate the combination of PTT and targeted-chemotherapy effects, the anticancer ability of DOX, $Cu_{39}S_{28}$/DOX, $Cu_{39}S_{28}$-FA/DOX in the same DOX concentrations from 6.25 to 100 μg/mL with or without NIR irradiation (808 nm, 1W/cm^2) were studied. As shown in Figure 5C, all groups co-cultured with MCF-7 cells show toxicity with the increase of DOX. It is worth mentioning that, the $Cu_{39}S_{28}$-FA/DOX + NIR combination group showed even higher toxicity on MCF-7 cells than other groups. For the over-expression of FA receptor in MCF-7 cells, the FA functionalized nanoparticles are more easily taken by these cells *via* receptor-mediated endocytosis.[43] In the $Cu_{39}S_{28}$-FA/DOX + NIR group, more nanoparticles were taken up by MCF-7 cells, the DOX release was quicker inside the cancer cells under NIR irradiation than the non-NIR treat group and more than 80% cells died in the experiments. The results proved that $Cu_{39}S_{28}$-FA/DOX can effectively be taken up by MCF-7 cancer cells and the DOX release efficacy can be significantly enhanced under NIR.

The hemolytic experiments were taken out with human red blood cells for the potential intravenous administration *in vivo*. No visual red color occurred in the $Cu_{39}S_{28}$ group with gradient concentrations, from 31.25 to 500 μg/mL and for the PBS group. The highest hemolytic efficiency with different particle concentration from 31.25 to 500 μg/mL is 0.071%, indicating that the as-prepared $Cu_{39}S_{28}$ HNPs are not hemolytic. The red color in pure water group was attributed to the hemoglobin from erythrocyte. In conclusion, the $Cu_{39}S_{28}$ HNPs were almost nontoxic to live cells and the as synthesized materials have good biocompatibility in blood.

2.5 Live/dead Staining

The anti-cancer effect of $Cu_{39}S_{28}$, $Cu_{39}S_{28}$-FA loaded with or without DOX nanocomposites under NIR irradiation (1 W/cm^2, 0 W/cm^2) was analyzed by live/dead staining. The live cells were dyed into green with calcein AM and dead cells were red with PI. As shown in Figure 6, the MCF-7 cells co-cultured with $Cu_{39}S_{28}$, $Cu_{39}S_{28}$-FA were almost all green, which was in accordance with the MTT results. At the same time, there was negligible absorbance at 808 nm in the medium so that the MCF-7 cells under NIR irradiation (1W/cm^2) were in a good state. Though the volumes of cell nucleus increased and the cell edges became vague in the free DOX treatment group (25 μg/mL, co-cultured for 24 h), there were still more than half number of cancer cells alive. While in the $Cu_{39}S_{28}$-FA/DOX + NIR group, all of the cells were dyed into red and completely dead, indicating the distinguished anti-cancer effects of targeted-chemo and photothermal synergistic effect.

2.6 Cell Apoptosis and Necrosis

Apoptosis is an important index for evaluation of cancer state due to its key effects in all tumor development.[44] As shown in Figure 7, there was almost no difference of apoptosis and necrosis in $Cu_{39}S_{28}$, $Cu_{39}S_{28}$-FA, NIR and the control groups, indicating negligible early apoptosis effects when employing nanocomposites or NIR separately. For the $Cu_{39}S_{28}$ +

NIR and $Cu_{39}S_{28}$-FA + NIR groups, 41.3 % and 78.6 % cells were induced to late apoptosis/necrosis. There were 48.7 % necrosis cells in the free DOX (25 μg/mL) treated group, while in $Cu_{39}S_{28}$/DOX + NIR and $Cu_{39}S_{28}$-FA/DOX + NIR groups, 55.91 % and 96.42 % late apoptosis/necrosis cells occurred. The flow cytometry data revealed that cells upon photothermal and chemotherapy treatment by $Cu_{39}S_{28}$-FA/DOX suffered irreversible damage, and the cells could no longer function or recover from the damage. Moreover, the FA modified nanocomposites were easily taken up *via* receptor mediated endocytosis by the FA receptor, so that the targeted photothermal treatment and chemotherapy work more efficiently inside the cells under the same conditions.

2.7 Targeted Effect *in Vitro*

Folic acid receptors (FRs) have been overexpressed in cancer cells, especially in breast cancers. In contrast, they are minimally distributed in normal tissues. They have served as an attractive target for tumor-specific drug delivery and therapy. In this research, we employed the flow cytometry to test the FITC labeling nanocomposites to test the targeted effect and enhanced cellular uptake of $Cu_{39}S_{28}$-FA nanoparticles. As shown in Figure 8, the mean fluorescein intensity of MCF-7 cells co-cultured with $Cu_{39}S_{28}$-FA (targeted group) was significantly enhanced ($p<0.01$), while the Control group, blocking group and $Cu_{39}S_{28}$ group exhibited negliable fluorescence enhancement. Successful FA targeting of $Cu_{39}S_{28}$-FA was demonstrated *in vitro*.

2.8 Biodistribution and Targeted Effect

To explore the targeted effect, distribution and dynamics of injected nanoparticles *in vivo*, nude mice bearing with MCF-7 tumor model were established. The nude mice (6~8 weeks old female Balb/c) were purchased from Medical Experimental Animal Center of Guangdong Province. All animal experiments were approved and performed in compliance with the local ethics committee and Guangzhou General Hospital of Guangzhou Military Command institutional guidelines.

$Cu_{39}S_{28}$, $Cu_{39}S_{28}$-FA nanoparticles and PBS were intravenous (*i.v.*) injected to the mice, the biodistribution of Cu^{2+} in tumor, muscles and main organs were analyzed by Inductively Coupled Plasma Mass Spectrometry (ICP-MS) after 24 h. Compared to the untargeted groups, ~10 times folate-conjugated nanoparticle concentrated in the tumor sites after administration 24 h, the results was in accordance with the flow cytometry results. More importantly, less Cu^{2+} in $Cu_{39}S_{28}$-FA group were observed in the main organs. In contrast, for $Cu_{39}S_{28}$ nanoparticles, the results (Figure S6) illustrated significantly higher Cu^{2+} contents in liver and spleen when compared with the PBS group ($p<0.01$) and targeted group ($p<0.05$) after 24 h injection, suggesting the metabolic pathway of the $Cu_{39}S_{28}$ nanoparticles are mainly through the liver and spleen, which was consistent with previous research.[45] Notably, the targeting nanoparticles exhibited enhanced antitumor activity and less toxicity to the body, attributed to the targeted effect at the tumor site as well as less nanoparticles and loading drugs accumulating in main organs.

2.9 *In Vivo* Targeted Photothermal and Chemo-Therapy Effect

The synthetic tumor ablation effect of $Cu_{39}S_{28}$-FA/DOX under 808 nm laser irradiation was analyzed for the further application. Following NIR irradiation, the temperature of breast tumors in mice was monitored by an infrared (IR) thermal camera (Figure 9). The temperature in tumor site reached up to 43 °C in $Cu_{39}S_{28}$-FA and $Cu_{39}S_{28}$-FA/DOX group. While in PBS and DOX group, the skin temperature only reached 35 °C, which is lower than the normal inner body temperature, illustrating tsafety under the 808 nm (1 W/cm^2) NIR laser. The results furhter confirmed the well targeted photothermal effect of the FA modified nanoparticles.

Then, as an important parameter of therapeutic effects, the change of tumor volume has been recorded from day 1 to day 14. As shown in Figure 10, the $Cu_{39}S_{28}$-FA/DOX exhibited a mild inhibition in tumor growth similar to the use of free DOX group without NIR irradiation, which may be ascribed to the targeted and pH-responsive effect of the nanocomposites in the first 4 days. However, the free DOX and $Cu_{39}S_{28}$-FA/DOX groups exhibited the same growth trend with control groups after 4 days, which could be caused by the drug-resistance of breast cancer. When with NIR irradiation, a clear shrink of tumor occured in both $Cu_{39}S_{28}$-FA and $Cu_{39}S_{28}$-FA/DOX group for the hypothermal effect. Notably, the tumor volume in $Cu_{39}S_{28}$-FA/DOX +NIR group reduced more than 90%, indicating the excellent combined photothermal and chemotherapy effects in tumor therapy. The DOX loading $Cu_{39}S_{28}$-FA groups showed the best tumor inhibition effect over the 14 days when compared with other groups. In addition, the change of body weight is also a major reference to assess systemic toxicity. Body mass loss in the treatment groups were not observed. In contrast, without suffering from the tumor, the body weight increased from 4 to 14 days after treatment in $Cu_{39}S_{28}$-FA/DOX+NIR group.

Hematein and Eosin (H&E) Staining—To further confirm the biocompatibility of the nanocomposites, the the representative hematein and eosin (H&E) staining images of the heart, liver, spleen, lung and kidney organs from the mice in different groups were displayed in Figure 11. There was no tissue damage or adverse effects in the treatment groups. The glomerulus structure was clear and complete in the kidney section of the treatment group, hepatocytes were normal and no pulmonary fibrosis or congestion, indicating the good biocompatiblity of $Cu_{39}S_{28}$-FA/DOX nanocomposites. In addition, the histology changes in the tumor were also studied. The tumors in PBS, NIR and $Cu_{39}S_{28}$-FA groups showed typical pathological characteristics of breast cancer and high clear vascular structure, demonstrating negligible effects of NIR or $Cu_{39}S_{28}$-FA upon the tumor. Serious damage in tumor cells can be found in the $Cu_{39}S_{28}$FA/DOX+NIR group, such as cell nucleus deformation, intercellular edema and all the tomor structure occured in a vague and in remarkable atrophie situation. The H&E staining of tumor tissues demonstrates that NIR illuminated DOX-loading nanocomposites can cause more severe tumor cell damage when compared with the other groups, which was consistent with the above results. Therefore, based on the excellent drug delivery ability and photothermal conversion effect, the nanocomposites can work as efficient anti-cancer nanoagents both in vitro and in vivo.

Conclusions

In summary, hollow $Cu_{39}S_{28}$ nanopeanuts have been synthesized by a facile one-step method and the formation mechanism has been investigated in detail. The unique nanopeanut $Cu_{39}S_{28}$ HNPs can work as splendid photothermal agents as well as drug loading carriers, and the release of DOX can be triggered by NIR and pH at the same time. The FA can conjugate with $Cu_{39}S_{28}$ HNPs directly without further surface modification, and a significantly higher accumulation of $Cu_{39}S_{28}$ HNPs in tumor cells and less accumulation in the main organs in $Cu_{39}S_{28}$-FA groups. When combined with NIR irradiation, the $Cu_{39}S_{28}$-FA/DOX nanocomposites presented serious toxicity on breast cancer cells, revealing synergistic chemotherapy and photothermal effect and showed better therapy effect than chemotherapy or photothermal therapy alone both *in vitro* and *in vivo*. The strong antitumor effectiveness of $Cu_{39}S_{28}$-FA/DOX can work as an excellent anticancer nanomedicine and would give a new way for anticancer nanomaterials development.

Supplementary Material

Refer to Web version on PubMed Central for supplementary material.

Acknowledgments

We acknowledge the financial support from the the financial support from the National Key Research Program of China (Grant No. 2016YFB0700803), National Natural Science Foundation of China (Grant Nos. 51672085, 81271957, 81501859, 81601884, 81402409), the Department of Education of Guangdong Province (Grant No. 2013gjhz0001), Fundamental Research Funds for the Central Universities, Key Program of Guangzhou Scientific Research Special Project, and Hundred, Thousand and Ten Thousand Leading Talent Project in Guangdong Program for Special Support of Eminent Professionals. Natural Science Foundation of Guangdong Province, China (Grant No. 2015A030312004), and Scientific and Technological Projects of Guangzhou, China (Grant No. 201604020110), the National Institutes of Health R01MH103133 and the Human Frontier Science RGY-0090/2014 (GH). In the end, we would appreciate very much Prof. Dr. Peter. A. Tanner for his helps to improve the language of the paper.

References

1. Hutchinson L. Nat Rev Clin Oncol. 2010; 7:669–670. [PubMed: 21116236]
2. Chen W, Zheng R, Zhang S, Zhao P, Zeng H, Zou X. Ann Transl Med. 2014; 2:61. [PubMed: 25333036]
3. Veronesi U, Cascinelli N, Mariani L, Greco M, Saccozzi R, Luini A, Aguilar M, Marubini E. New Engl J Med. 2002; 347:1227–1232. [PubMed: 12393819]
4. Zhao Z, Chan PS, Li H, Wong KL, Wong RN, Mak NK, Zhang J, Tam HL, Wong WY, Kwong DW. Inorg Chem. 2012; 51:812–821. [PubMed: 22191427]
5. Chan CF, Tsang MK, Li H, Lan R, Chadbourne FL, Chan WL, Law GL, Cobb SL, Hao J, Wong WT. J Mater Chem B. 2013; 2:84–91.
6. Zhang J, Wong KL, Wong WK, Mak NK, Kwong DW, Tam HL. Org Biomol Chem. 2011; 9:6004–6010. [PubMed: 21748193]
7. Yao M, Ma L, Li L, Zhang J, Lim RX, Chen W, Zhang Y. J Biomed Nano. 2016; 12:1835–1851.
8. Zhang H, Wei Z, Yong Z, Jiang Y, Li S. Transl Oncol. 2017; 10:229–240. [PubMed: 28193559]
9. Li L, Rashidi LH, Yao M, Ma L, Chen L, Zhang J, Zhang Y, Chen W. Photodiagn Photodyn. 2017
10. Liu B, Li C, Cheng Z, Hou Z, Huang S, Lin J. Biomater Sci. 2016; 4:890–909. [PubMed: 26971704]
11. Jaque D, Martinez Maestro L, del Rosal B, Haro-Gonzalez P, Benayas A, Plaza JL, Martin Rodriguez E, Garcia Sole J. Nanoscale. 2014; 6:9494–9530. [PubMed: 25030381]

12. Wang S, Huang P, Nie L, Xing R, Liu D, Wang Z, Lin J, Chen S, Niu G, Lu G. Adv Mater. 2013; 25:3055–3061. [PubMed: 23404693]
13. Park H, Yang J, Seo S, Kim K, Suh J, Kim D, Haam S, Yoo KH. Small. 2008; 4:192–196. [PubMed: 18203232]
14. Austin LA, Mackey MA, Dreaden EC, El-Sayed MA. Arch Toxicol. 2014; 88:1391–1417. [PubMed: 24894431]
15. Yan L, Qiu L. Nanomedicine. 2015; 10:361–373. [PubMed: 25707973]
16. Zhao Y, Song W, Wang D, Ran H, Wang R, Yao Y, Wang Z, Zheng Y, Li P. ACS Appl Mater Inter. 2015; 7:14231–14242.
17. Li Y, Lu W, Huang Q, Huang M, Li C, Chen W. Nanomedicine. 2010; 5:1161–1171. [PubMed: 21039194]
18. Tian Q, Jiang F, Zou R, Liu Q, Chen Z, Zhu M, Yang S, Wang J, Wang J, Hu J. ACS Nano. 2011; 5:9761–9771. [PubMed: 22059851]
19. Liu X, Fu F, Xu K, Zou R, Yang J, Wang Q, Liu Q, Xiao Z, Hu J. J Mater Chem B. 2014; 2:5358.
20. Zha Z, Zhang S, Deng Z, Li Y, Li C, Dai Z. Chem Commun. 2013; 49:3455–3457.
21. Forrest ML, Kwon GS. Adv Drug Deliver Rev. 2008; 60:861–862.
22. Zheng B, Gong X, Wang H, Wang S, Wang H, Li W, Tan J, Chang J. Nanotechnology. 2015; 26:425102. [PubMed: 26422130]
23. Holken I, Neubuser G, Postica V, Bumke L, Lupan O, Baum M, Mishra YK, Kienle L, Adelung R. ACS Appl Mater Inter. 2016; 8:20491–20498.
24. Yin Y, Rioux RM, Erdonmez CK, Hughes S, Somorjai GA, Alivisatos AP. Science. 2004; 304:711–714. [PubMed: 15118156]
25. Li J, Zeng HC. J Am Chem Soc. 2007; 129:15839–15847. [PubMed: 18047331]
26. Li B, Xie Y, Xue Y. J Phys Chem C. 2007; 111:12181–12187.
27. Ma M, Chen H, Chen Y, Wang X, Chen F, Cui X, Shi J. Biomaterials. 2012; 33:989–998. [PubMed: 22027594]
28. You J, Zhang R, Zhang G, Zhong M, Liu Y, Van Pelt CS, Liang D, Wei W, Sood AK, Li C. J Control Release. 2012; 158:319–328. [PubMed: 22063003]
29. Ma M, Chen H, Chen Y, Wang X, Chen F, Cui X, Shi J. Biomaterials. 2012; 33:989–998. [PubMed: 22027594]
30. Chen F, Hong H, Goel S, Graves SA, Orbay H, Ehlerding EB, Shi S, Theuer CP, Nickles RJ, Cai W. ACS Nano. 2015; 9:3926–3934. [PubMed: 25843647]
31. Lv R, Yang P, He F, Gai S, Yang G, Lin J. Chem Mater. 2015; 27:483–496.
32. Chen F, Hong H, Goel S, Graves SA, Orbay H, Ehlerding EB, Shi S, Theuer CP, Nickles RJ, Cai W. ACS Nano. 2015; 9:3926–3934. [PubMed: 25843647]
33. Tuteja B, Moniruzzaman M, Sundararajan PR. Langmuir. 2007; 23:4709–4711. [PubMed: 17378594]
34. Vlakh EG, Grachova EV, Zhukovsky DD, Hubina AV, Mikhailova AS, Shakirova JR, Sharoyko VV, Tunik SP, Tennikova TB. Sci Rep. 2017; 7:41991. [PubMed: 28155880]
35. Baláž M, Baláž P, Tjuliev G, Zubrík A, Sayagués MJ, Zorkovská A, Kostova N. J Mater Sci. 2012; 48:2424–2432.
36. Ahmed M, Goldberg SN. Inter J Hyperther. 2004; 20:781–802.
37. Chen P, Wang Z, Zong S, Zhu D, Chen H, Zhang Y, Wu L, Cui Y. Biosens Bioelectron. 2016; 75:446–451. [PubMed: 26360244]
38. Chen G, Shen J, Ohulchanskyy TY, Patel NJ, Kutikov A, Li Z, Song J, Pandey RK, Agren H, Prasad PN, Han G. ACS Nano. 2012; 6:8280–8287. [PubMed: 22928629]
39. Greco F, Vicent MJ, Gee S, Jones AT, Gee J, Nicholson RI, Duncan R. J Control Release. 2007; 117:28–39. [PubMed: 17129632]
40. Ramadan S, Guo L, Li Y, Yan B, Lu W. Small. 2012; 8:3066–3066.
41. Chang B, Guo J, Liu C, Qian J, Yang W. J Mater Chem. 2010; 20:9941–9947.
42. Chen L, Li L, Zhang L, Xing S, Wang T, Wang YA, Wang C, Su Z. ACS Appl Mater Inter. 2013; 5:7282–7290.

43. Pan D, Turner JL, Wooley KL. Chem Commun. 2003:2400.
44. Evan GI, Vousden KH. Nature. 2001; 411:342–348. [PubMed: 11357141]
45. Guo L, Panderi I, Yan DD, Szulak K, Li Y, Chen YT, Ma H, Niesen DB, Seeram N, Ahmed A, Yan B, Pantazatos D, Lu W. ACS Nano. 2013; 7:8780–8793. [PubMed: 24053214]

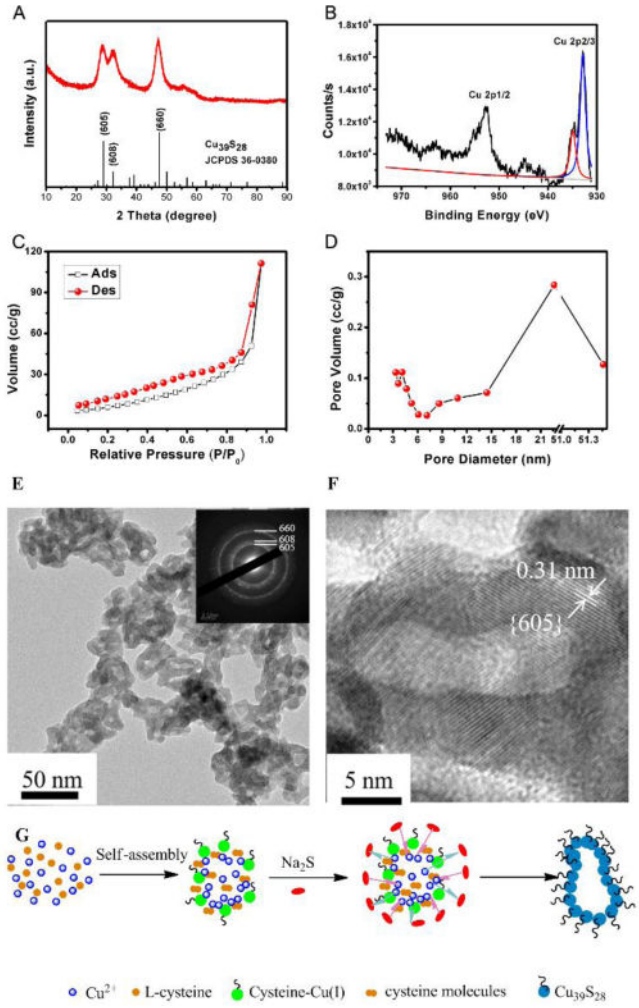

Figure 1.

(A) The XRD image of $Cu_{39}S_{28}$ HNPs; (B) XPS spectra of Cu 2p (Cu $2p_{1/2}$ and Cu $2p_{2/3}$ peak fit); The Cu $2p_{2/3}$ peak fit reveals a 2 peaks at 932.2 eV (corresponded to Cu^{+} in Cu(I)cysteine) and 933.5 eV (assigned to Cu^{2+} in CuS), corresponding well with the XRD results ($Cu_{39}S_{28}$); (C) Nitrogen adsorption/desorption isotherms; (D) Pore size distributions; (E) TEM images of as prepared $Cu_{39}S_{28}$ HNPs; Inset images: SAED of the $Cu_{39}S_{28}$ HNPs; (F) The interplanar crystal spacing of $Cu_{39}S_{28}$ HNPs; (G) Schematic illustration formation mechanism of $Cu_{39}S_{28}$ hollow nanopeanuts.

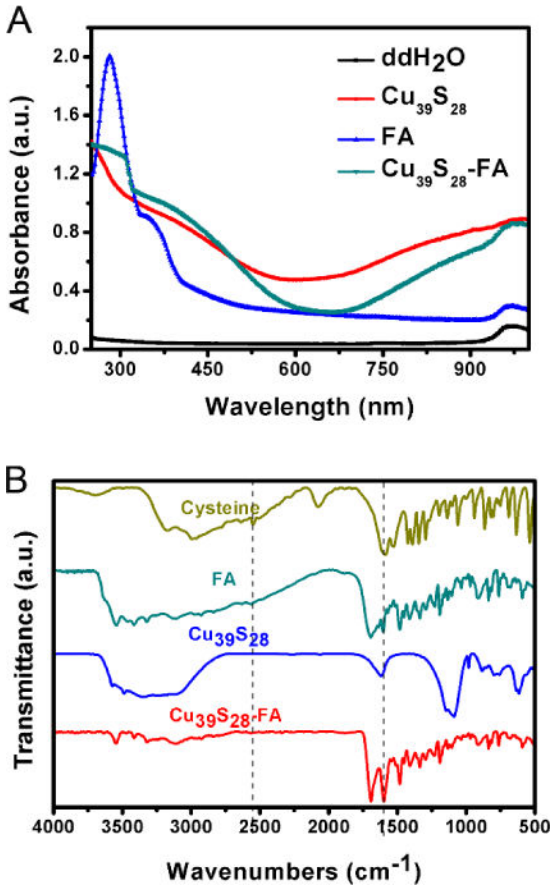

Figure 2.
(A) UV-VIS spectrum of different samples; (B) FTIR spectrums of different samples.

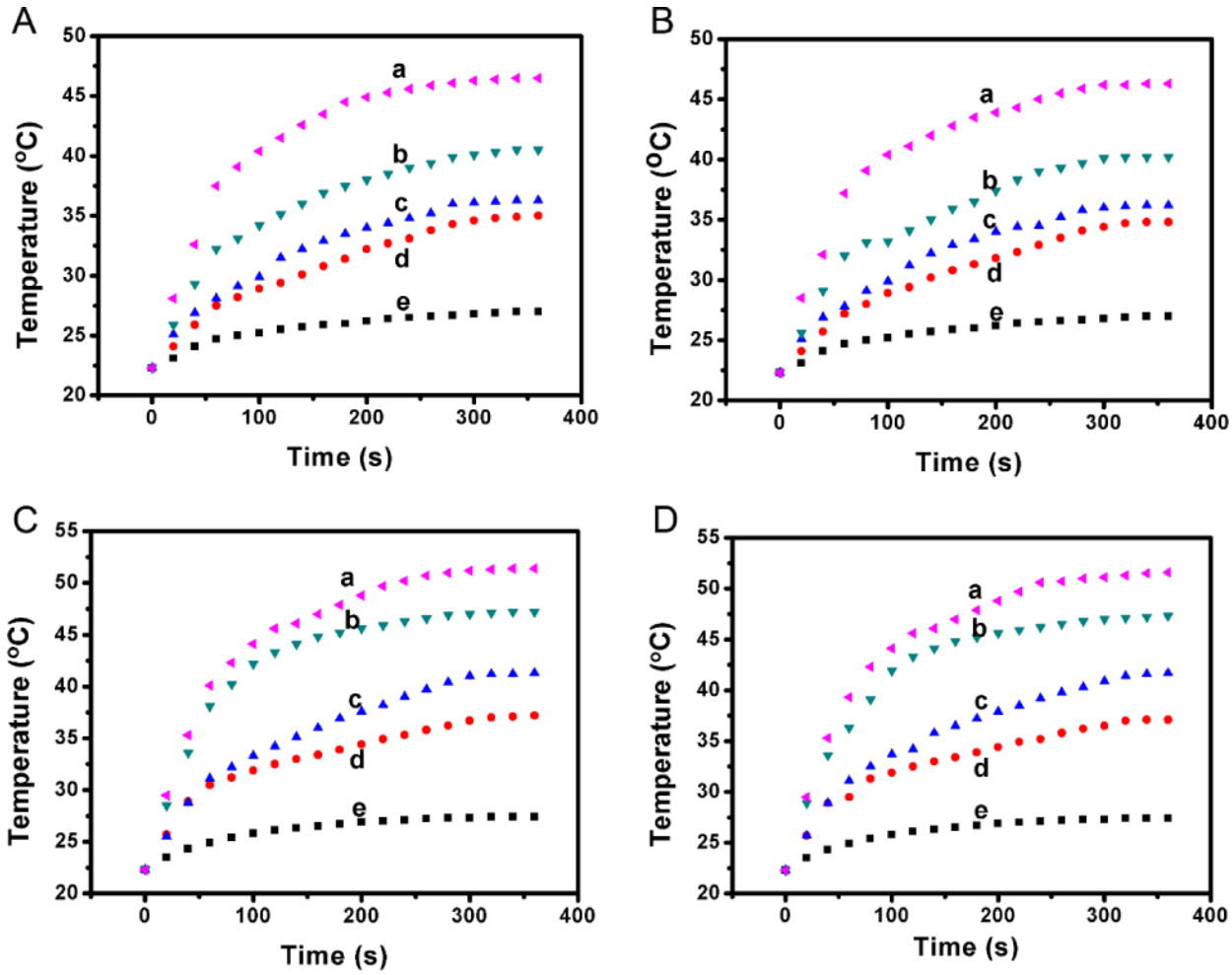

Figure 3.

Photothermal effect study of $Cu_{39}S_{28}$ and $Cu_{39}S_{28}$-FA nanoparticles. Quantitative temperature change of (A) $Cu_{39}S_{28}$ solutions at a density of 0.5 W/cm^2; (B) $Cu_{39}S_{28}$-FA solutions at a density of 0.5 W/cm^2; (C) $Cu_{39}S_{28}$ solutions at a density of 1 W/cm^2; (D) $Cu_{39}S_{28}$-FA solutions at a density of 1 W/cm^2 with 808 nm laser. Inset images shows the temperature change for samples with varied concentrations, a, b, c, d, e inserted in the figures means 1000, 500, 250, 125 and 0 μg/mL $Cu_{39}S_{28}$ or $Cu_{39}S_{28}$-FA, respectively.

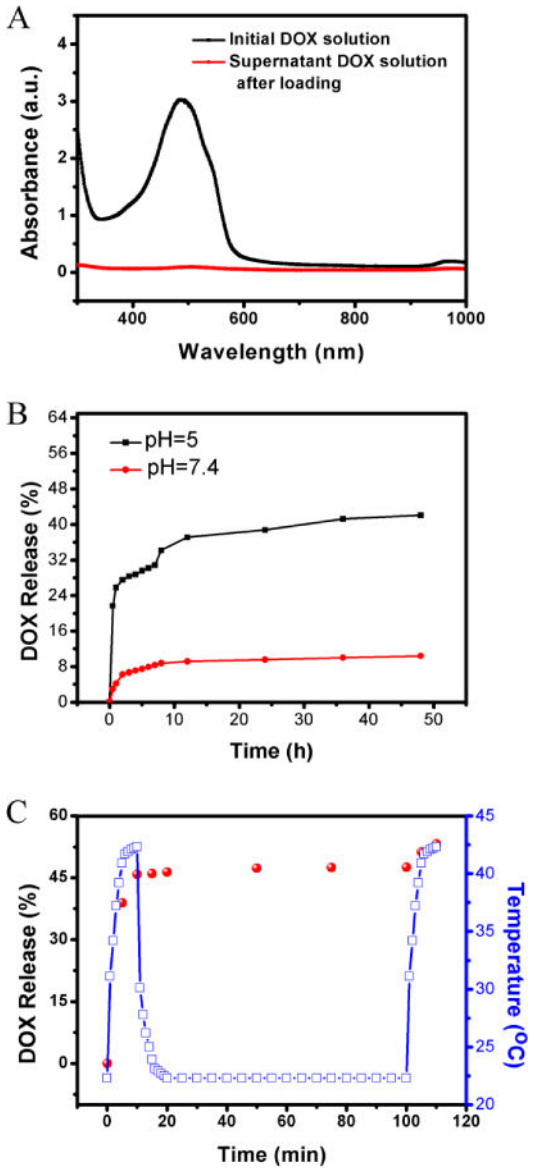

Figure 4.

The pH and NIR-dependent release behavior of DOX. (A)The absorption spectrum of DOX before and after mixing with $Cu_{39}S_{28}$ HNPs; (B) DOX-release profiles of DOX-loaded $Cu_{39}S_{28}$-FA nanoparticles measured at pH 5.0 and pH 7.4 in PBS buffer at room temperature; (C) NIR-triggered release of DOX from $Cu_{39}S_{28}$-FA/DOX nanocomposites with temperature change. The samples were irradiated with an 808 nm NIR laser from 0–10 min and the laser turned off, then recycled in 100–110 min.

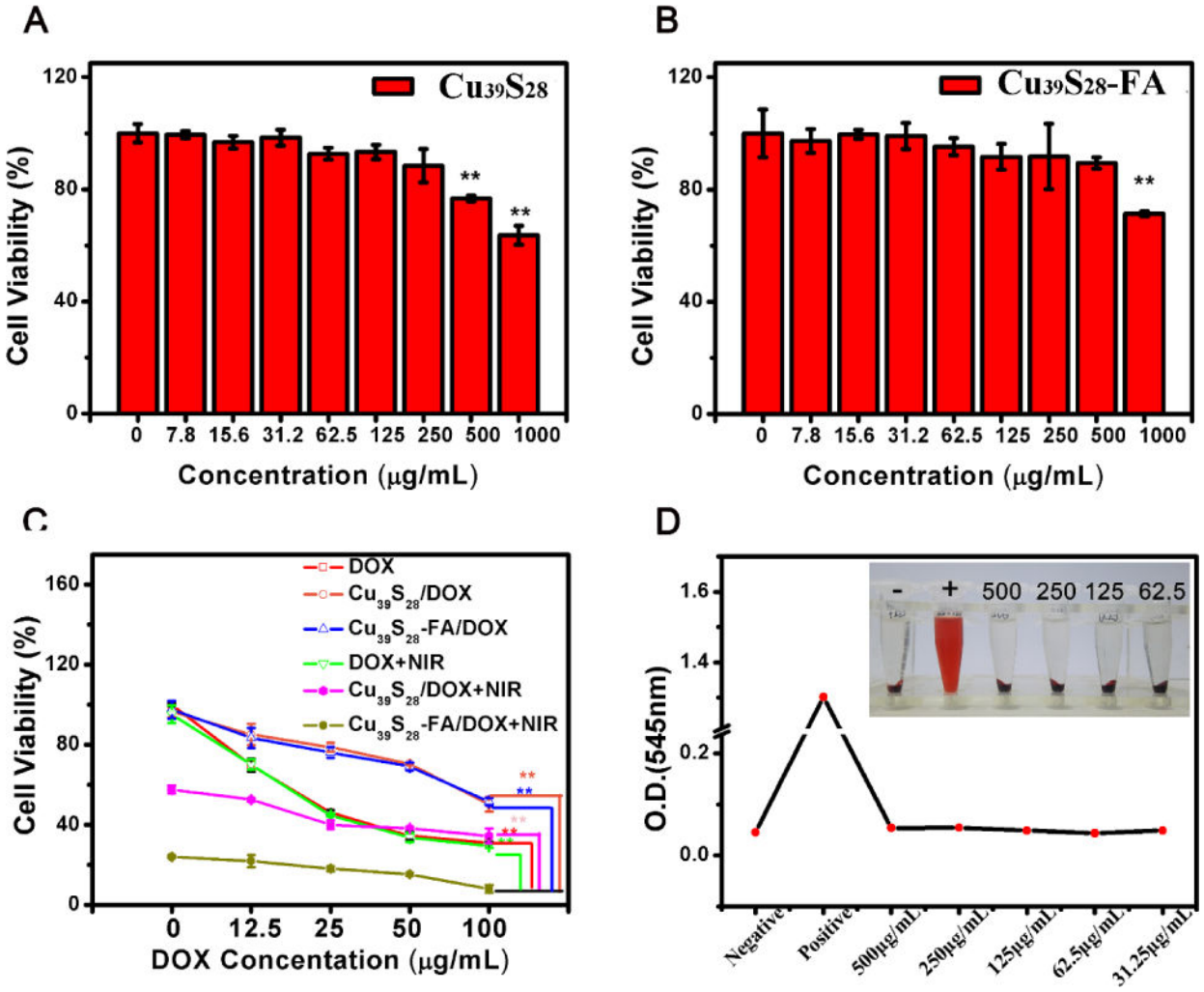

Figure 5.

Cytotoxicity and therapeutic effect evaluation of the nanocomposites by MTT assays. (A) *In vitro* cytotoxicity of MCF-7 cells exposed to different concentrations of $Cu_{39}S_{28}$ HNPs in DMEM for 24 h at 37 °C incubation; (B) *In vitro* cytotoxicity of MCF-7 cells exposed to different concentrations of $Cu_{39}S_{28}$-FA nanocomposites in DMEM for 24 h at 37 °C incubation; (C) *In vitro* cytotoxicity of MCF-7 cells exposed to different groups with varied DOX concentrations;1 DOX, 2 $Cu_{39}S_{28}$/DOX, 3 $Cu_{39}S_{28}$/DOX-FA/DOX, 4 $Cu_{39}S_{28}$/DOX +NIR, 5 $Cu_{39}S_{28}$/DOX-FA/DOX +NIR; (D)The hemolytic percentage of $Cu_{39}S_{28}$ HNPs to human red blood cells. *$p<0.05$, **$p<0.01$ with control group.

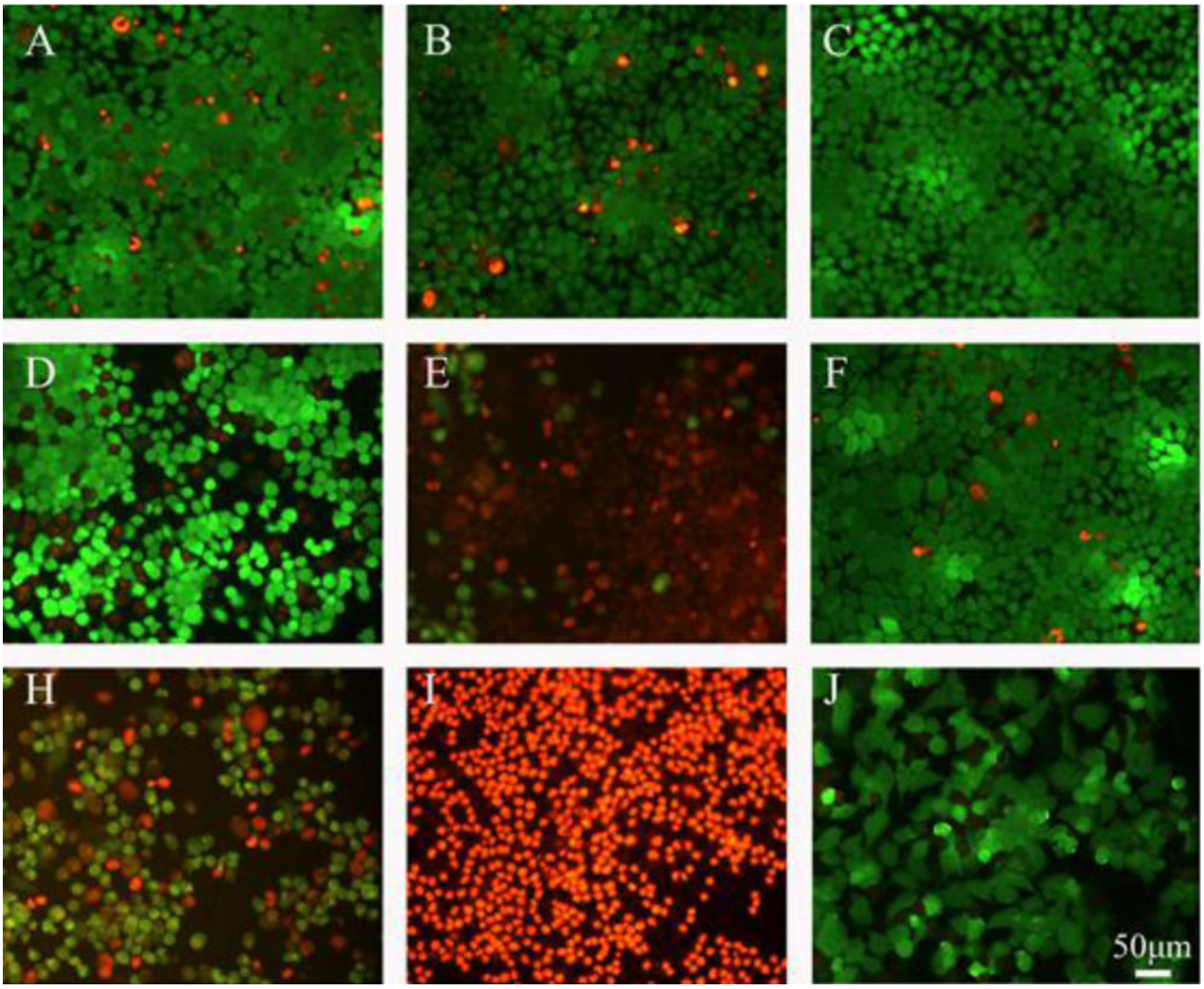

Figure 6.

Fluorescence micrographs of live/dead dye-stained MCF-7 cells after being cultured with different groups with or without 808 nm (1W/cm^2, 10min) NIR. (A) $Cu_{39}S_{28}$; (B) $Cu_{39}S_{28}$-FA; (C) Control; (D) $Cu_{39}S_{28}$+NIR; (E) $Cu_{39}S_{28}$-FA+NIR; (F) NIR; (H) $Cu_{39}S_{28}$/DOX +NIR; (I) $Cu_{39}S_{28}$-FA/DOX+NIR; (J) DOX. The concentration of DOX in all groups is 25 μg/mL. The scar scale =50 μm.

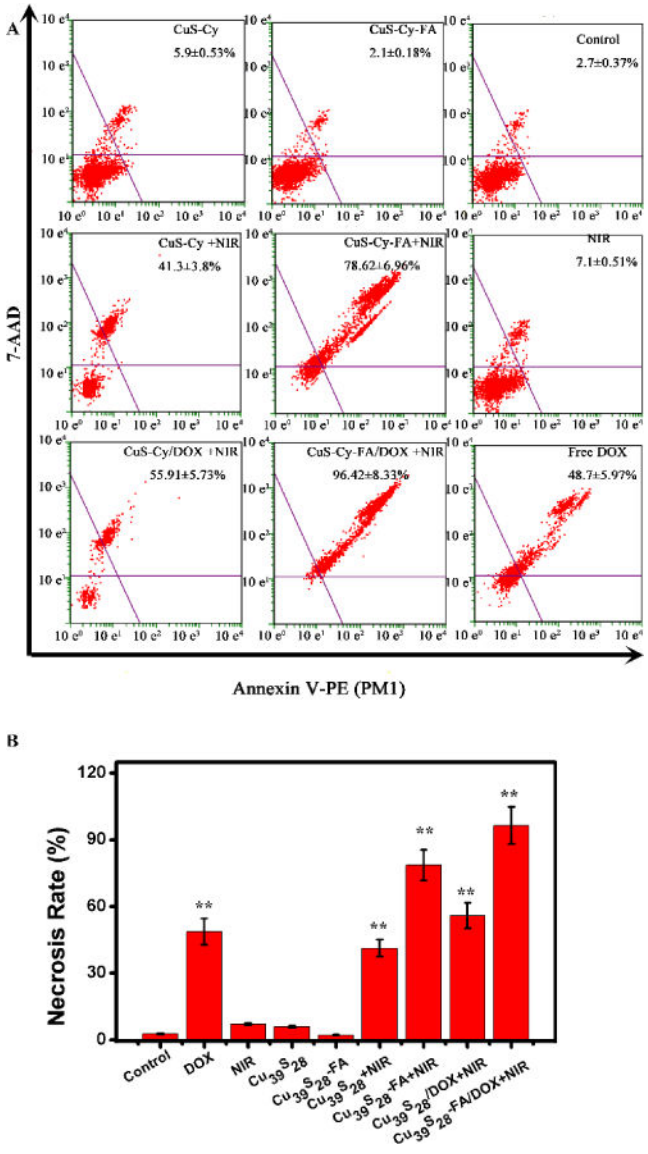

Figure 7.

The apoptosis and necrosis of MCF-7 cells after being co-cultured with different groups for 24 h with or without 808 nm (1 W/cm^2) NIR. (A) $Cu_{39}S_{28}$ (B) $Cu_{39}S_{28}$-FA; (C) Control; (D) $Cu_{39}S_{28}$+NIR; (E) $Cu_{39}S_{28}$-FA+NIR; (F) NIR; (H) $Cu_{39}S_{28}$/DOX+NIR; (I) $Cu_{39}S_{28}$-FA/DOX+NIR; (J) DOX. The concentration of DOX in all groups is 25 μg/mL.

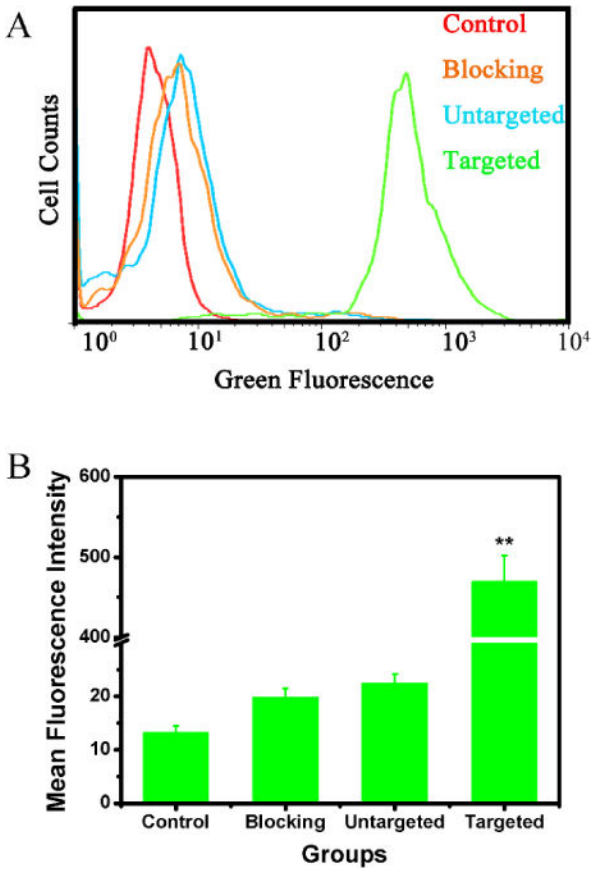

Figure 8.

Flow cytometry analysis of the targeted effect of $Cu_{39}S_{28}$-FA nanocomposites in MCF-7 (FA receptor positive) cell lines. (A) Flow cytometry studies on MCF-7 cells treated with different groups; (B) Fluorescence Intensity of different groups based on (A) (*$p<0.05$, **$p<0.01$ with control group).

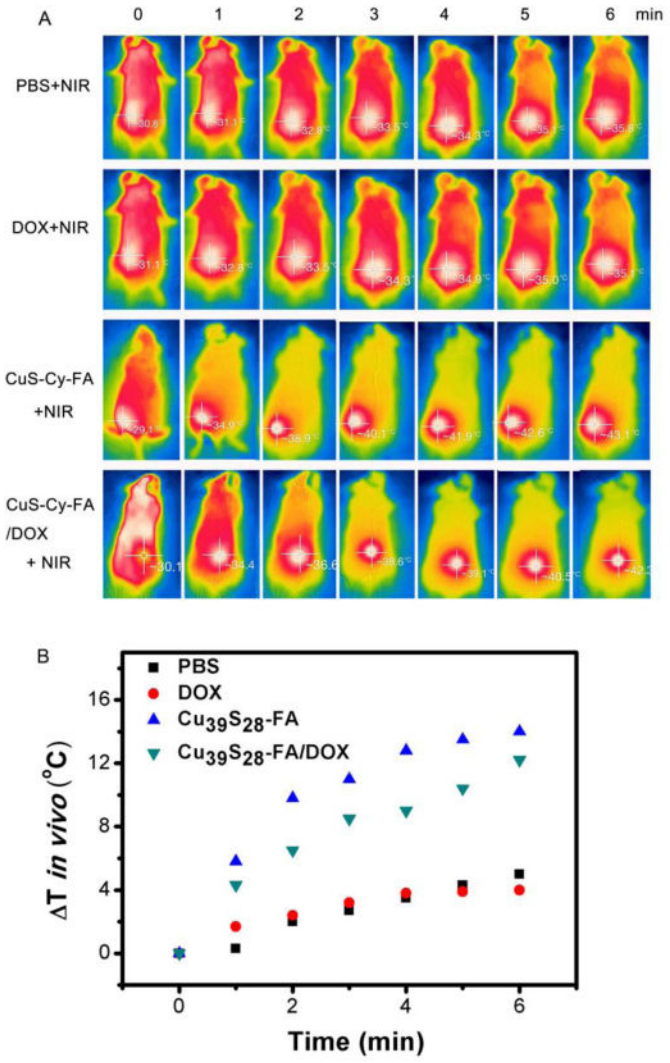

Figure 9.

(A) Infrared thermal images of tumor-bearing mice exposed (or not exposed) to NIR laser after intravenous injection with PBS, free DOX, $Cu_{39}S_{28}$-FA, $Cu_{39}S_{28}$-FA/DOX. (B) Temperature change curve of different groups *in vivo.*

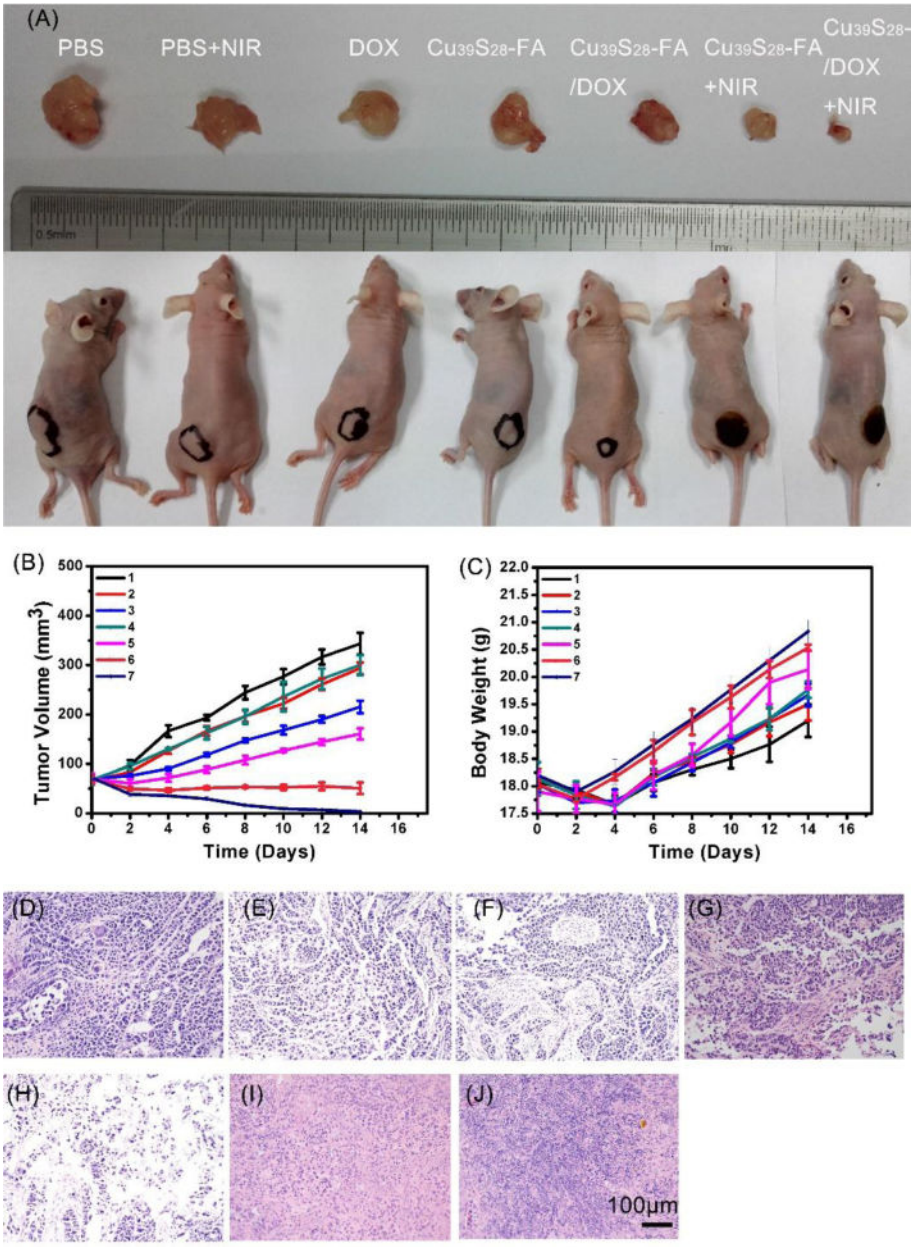

Figure 10.

(A) Photographs of tumor bearing mice and excised tumors after different treatments after 14 days; (B) Tumor volume growth curves of nude mice in different groups after various treatments;1 PBS, 2 PBS, 3 DOX, 4 $Cu_{39}S_{28}$-FA, 5 $Cu_{39}S_{28}$-FA/DOX, 6 $Cu_{39}S_{28}$-FA+NIR, 7 $Cu_{39}S_{28}$-FA/DOX+NIR; (C) Body weight change curves of nude mice in different groups after various treatments, 1 PBS, 2 PBS+NIR, 3 DOX, 4 $Cu_{39}S_{28}$-FA, 5 $Cu_{39}S_{28}$-FA/DOX, 6 $Cu_{39}S_{28}$-FA+NIR, 7 $Cu_{39}S_{28}$-FA/DOX+NIR; H&E staining images of tumor section after 14 days treatment in different groups from (D) DOX; (E) PBS+NIR ; (F) DOX ; (G) $Cu_{39}S_{28}$-FA ; (H) $Cu_{39}S_{28}$-FA/DOX; (I) $Cu_{39}S_{28}$-FA+NIR; (J) $Cu_{39}S_{28}$-FA/DOX+NIR.

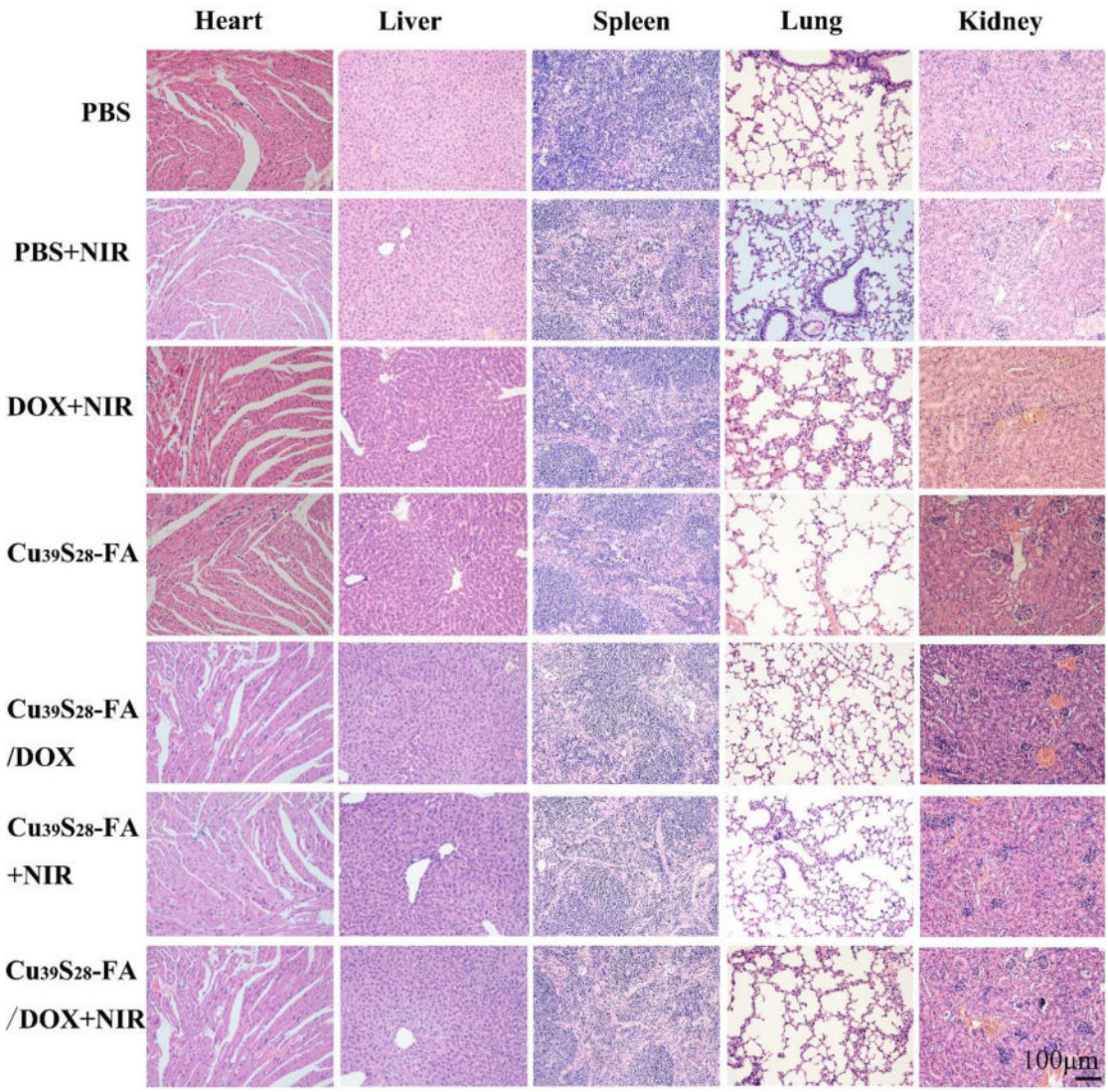

Figure 11.
H&E staining of the main organs in different treatment groups after 14 days.

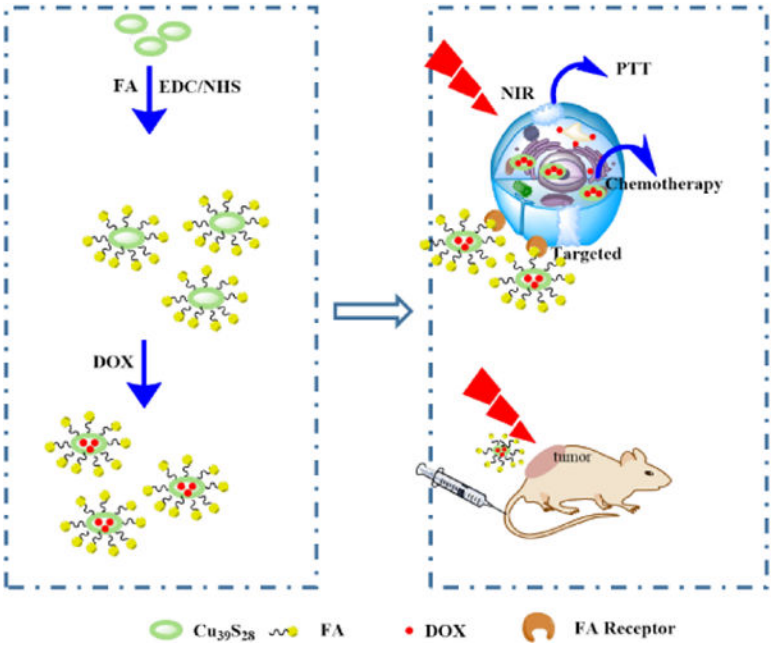

Scheme 1.

Schematic illustration of the synthetic process and targeted photothermal, chemotherapy of $Cu_{39}S_{28}$ hollow nanoparticles *in vitro* and *in vivo*.